SMALL SCALE DISCHARGE STUDIES

J. H. Jacob and J. A. Mangano
Avco Everett Research Laboratory, Inc.
2385 Revere Beach Parkway
Everett MA 02149

Semi–Annual Report for Period 1 March 1975 to 31 August 1975

Sponsored by

DEFENSE ADVANCED RESEARCH PROJECTS AGENCY
DARPA Order No. 1806

Monitored by

OFFICE OF NAVAL RESEARCH
DEPARTMENT OF THE NAVY
Arlington VA 22217

FOREWORD

DARPA Order No.: 1806

Program Code No.: 5E20

Name of Contractor: Avco Everett Research Laboratory, Inc.

Effective Date of Contract: 15 August 1974

Contract Expiration Date: 14 August 1976

Amount of Contract: $429,588

Contract No.: N00014-75-C-0062

Principal Investigator and Phone No.: J.H. Jacob
(617) 389-3000, Ext. 329

Scientific Officer: Director, Physics Program, Physical Sciences Div.
Office of Naval Research
Department of the Navy
800 North Quincy Street
Arlington, VA 22217

Short Title of Work: Laser Discharge Studies

UNCLASSIFIED

SECURITY CLASSIFICATION OF THIS PAGE *(When Date Entered)*

REPORT DOCUMENTATION PAGE

READ INSTRUCTIONS BEFORE COMPLETING FORM

1. REPORT NUMBER	2. GOVT ACCESSION NO.
3. RECIPIENT'S CATALOG NUMBER	
4. TITLE (and Subtitle) Small Scale Discharge Studies	5. TYPE OF REPORT & PERIOD COVERED Semi-Annual Report 1 March 1975 – 31 Aug. 1975
6. PERFORMING ORG. REPORT NUMBER	
7. AUTHOR(s) J. H. Jacob and J. A. Mangano	8. CONTRACT OR GRANT NUMBER(s) N00014-75-C-0062
9. PERFORMING ORGANIZATION NAME AND ADDRESS Avco Everett Research Laboratory, Inc. 2385 Revere Beach Parkway Everett, MA 02149	10. PROGRAM ELEMENT, PROJECT, TASK AREA & WORK UNIT NUMBERS DARPA, Order – 1806
11. CONTROLLING OFFICE NAME AND ADDRESS Defense Advanced Research Projects Agency DARPA Order No. 1806	12. REPORT DATE 31 Aug 75
	13. NUMBER OF PAGES 41
14. MONITORING AGENCY NAME & ADDRESS *(if different from Controlling Office)* Office of Naval Research Department of the Navy Arlington, VA 22217	15. SECURITY CLASS. *(of this report)* Unclassified
	15a. DECLASSIFICATION/DOWNGRADING SCHEDULE

16. DISTRIBUTION STATEMENT *(of this Report)*

Approved for Public Release; Distribution Unlimited.

41 p.

17. DISTRIBUTION STATEMENT *(of the abstract entered in Block 20, if different from Report)*

18. SUPPLEMENTARY NOTES

19. KEY WORDS *(Continue on reverse side if necessary and identify by block number)*

Visible/UV Lasers
High Pressure Discharges
Rare Gas Fluoride Lasers
KrF^* Laser

20. ABSTRACT *(Continue on reverse side if necessary and identify by block number)*

Laser action has been obtained in atmospheric-pressure mixtures containing ≈95% Ar ≈ 5% Kr and ≤ 0.3% F_2 by e-beam controlled discharge pumping. The physics of these discharges are dominated by electron impact excitation and ionization of the rare gas metastables. The ionization of the metastables impacts the discharge stability directly while their excitation strongly effects the efficiency of producing KrF^*. Hence, two step ionization is dominant. For stable equilibrium, the attachment rate has to be greater than or equal to twice the ionization rate. Under stable discharge conditions, the metastable

DD FORM 1 JAN 73 1473 EDITION OF 1 NOV 63 IS OBSOLETE

UNCLASSIFIED

SECURITY CLASSIFICATION OF THIS PAGE *(When Date Entered)*

048450

(20)
production efficiency can be as high as 70% and the KrF* production efficiency 35%.

REPORT SUMMARY

During the period from March 1975 - August 1975 we have designed and fabricated a high pressure e-beam controlled discharge cavity. Following the discovery of the KrF* laser by pure e-beam pumping, laser action in an e-beam controlled discharge was obtained in May 1975. We have also investigated the possibility of building a NO γ-band laser.

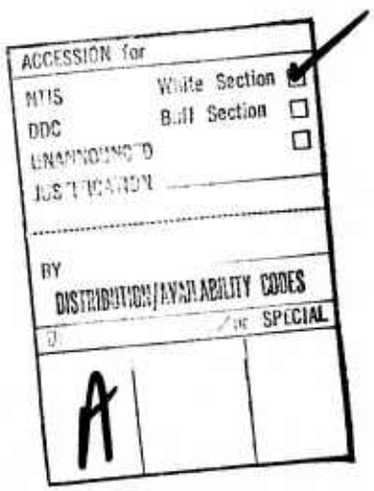

TABLE OF CONTENTS

LIST OF ILLUSTRATIONS

I. E-BEAM STABILIZED DISCHARGE EXPERIMENT

The e-beam stabilized discharge apparatus is composed of four major parts.

(1) Electron Gun

(2) Laser/Discharge Cavity

(3) Discharge Circuitry

(4) Diagnostics

In this section these components will be described.

1. ELECTRON GUN

Under a previous ARPA/MICOM contract, a cold cathode electron gun was developed. A cross-sectional diagram of the electron gun is given in Figure 1. This gun produces an e-beam having an energy of 150 keV, a current density of 20 A/cm^2, a pulse length of 125 or 250 nsec and a cross-sectional area of 10 cm x 25 cm.* Oscillograms of the gun voltage and current are given in Figure 2. The uniformity of the e-beam current density over its cross-sectional area was shown to be within $\pm$ 5% through the use of standard blue cellophane/spot densitometry techniques. These measurements were made at the gun anode where the beam current had not been smoothed by scattering in the foil or gas. Beam current densities in the range between 0.1 and 20 A/cm^2 can easily be extracted from this gun by using beam attenuator screens. Therefore, this gun was readily adaptable to provide a wide range of preionization levels for e-beam stabilized discharge research.

* Under the FY 75 Laser Discharge Studies contract a new cathode for this gun was designed so that an e-beam with a current density up to 50 A/cm^2 and a cross-sectional area of 2.5 cm x 25 cm can be produced.

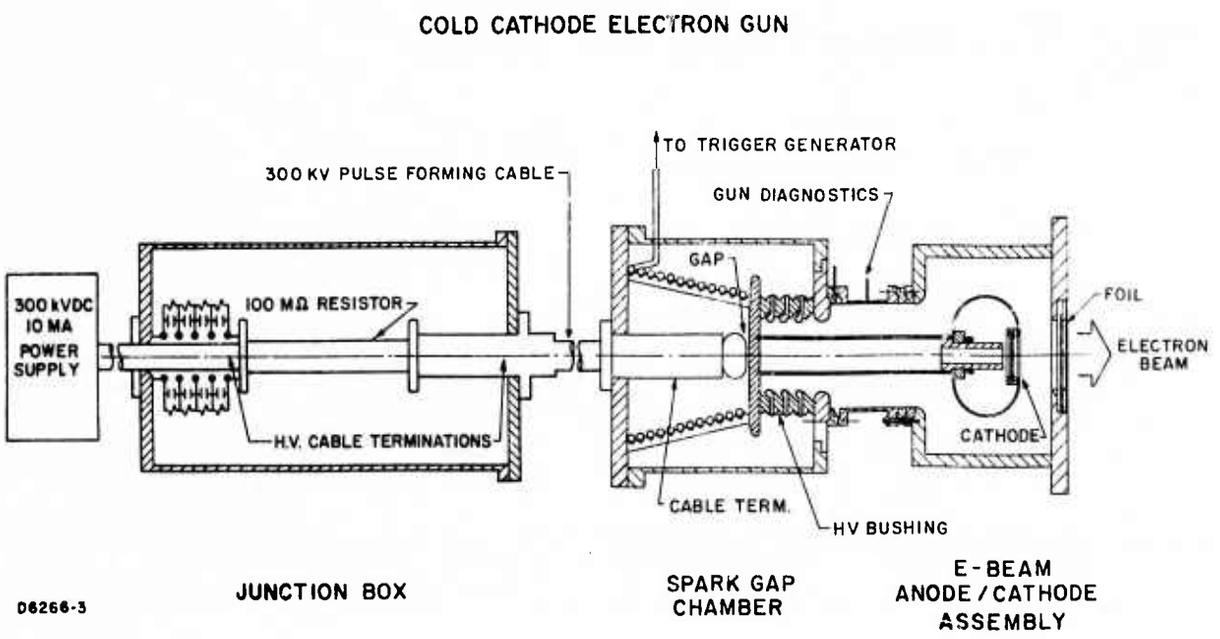

Figure 1 Schematic of Electron Gun

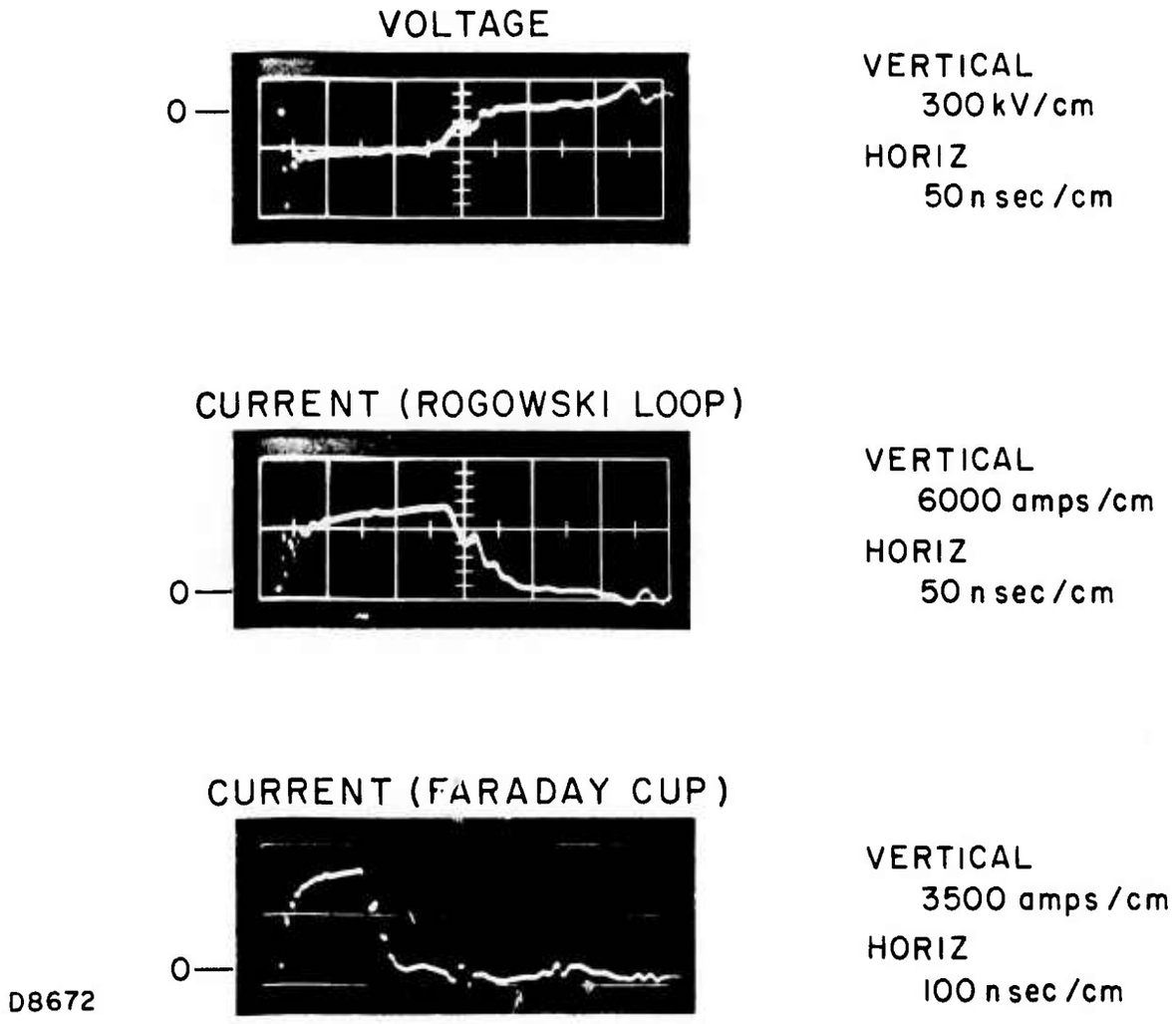

Figure 2 Electron Gun Voltage-Current Characteristics with a Graphite Cathode

The design and operation of this gun represents an important step in cold cathode electron gun research and its applications to the development of efficient, high power visible lasers. This is true for two reasons. First the gun is efficient. Nearly all (90%) of the energy stored in the pulse forming cable is converted into e-beam energy at 150 keV. This efficiency is achieved because of the inherently rapid turn on/turn off characteristics of the pulse forming cable. Effectively all of the beam electrons leaving the cathode are accelerated through the full anode-to-cathode potential so that beam energy losses in the foil are minimized. This condition will be especially important when repetitive pulsing of the electron gun becomes important. One of the main limitations on the repetition rate (and hence average power) of a laser is associated with limits on the foil cooling capability. Therefore, efforts at minimizing foil heating are rewarded directly in increased average laser power capability.

The second advantage of this electron gun design is its simplicity. Only one spark gap is involved so that the gun is readily multiply-pulsed at high rep rate (with the addition of spark gap gas flow and a higher current 300 kV DC power supply). Therefore, only the foil cooling capability developed under the AERL CO_2 laser programs must be adapted to give high rep rate, efficient gun performance.

2. LASER/DISCHARGE CAVITY

The existing discharge cavity is shown schematically in Figure 3. This cavity was designed so that intrinsic discharge/laser performance could be accurately observed on a small scale without complications arising from e-beam scattering, etc.

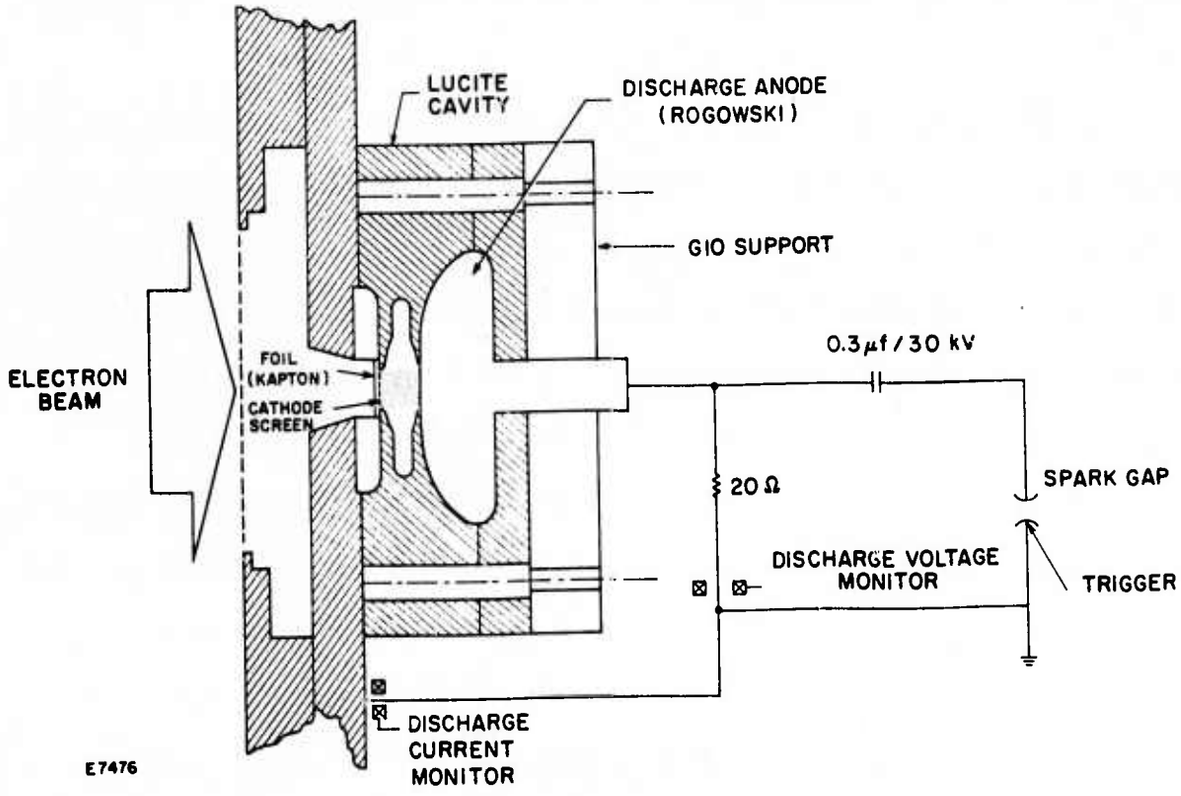

Figure 3 E-beam Stabilized Discharge Experiment

The suitably-attenuated e-beam enters this cavity from vacuum through an 80% open foil support structure and a 1 to 2 mil thick kapton foil. The beam then passes through a grounded s.s. wire mesh of variable transmittance (which serves as the discharge cathode) and preionizes the laser mixture. The beam is collected on an s.s. Rogowski-shaped discharge anode.

Optical access to the 2 cm x 2 cm x 20 cm discharge cavity is provided by quartz windows aligned at Brewster's angle to the long dimension of the cavity. Two aluminum mirror mount supports are rigidly attached to the massive s.s. plate forming one end of the electron beam vacuum chamber. The sidewalls of the cavity box are machined from lucite. A G10 backplate provides additional support so that the cavity can support laser mixture pressures of up to 3 atmospheres. A LN_2 baffled, 2" diffusion pump system is used to establish a cavity base pressure of $\leq 10^{-5}$ torr. An all stainless steel gas manifolding system has been built so that up to three gases can be mixed in situ in the laser cavity. The experiment is housed in a room compatible with the use of toxic gases.

3. DISCHARGE CIRCUITRY

A low inductance ($\sim$120 nh overall) capacitive discharge circuit is used to pulse the anode positively with respect to the cathode as shown in Figure 3. A specially designed trigatron spark gap, with a jitter time less than 10 nsec and a separate HV trigger generator, is used to switch the 0.1 μf capacitor (90 kV DC) across the discharge electrodes. In this manner, the delay between the firing of the discharge and the e-beam can be independently controlled. A series 2 Ω resistor is used to absorb most of the capacitor

energy after an arc occurs and prevent damage to the cavity. The 20 Ω shunt resistor serves two purposes. First it damps oscillations in discharge voltage (and current) caused by stray circuit capacitance and inductance. This ringing can produce an undesired overshoot in the initial discharge voltage (and lead to premature arcing) under conditions of high initial discharge resistance. This 20 Ω resistor is also used as part of the discharge voltage monitor. The current through this resistor is monitored by a calibrated current transformer. The product of current and resistance then gives the voltage across the discharge electrodes as a function of time. This novel method of measuring discharge voltage was developed because standard voltage divider techniques (resistive or capactive) were found to be unreliable and/or noisy.

With the circuitry described above discharge energy inputs of up to 1 kJ/liter at electric fields of up to 40 kV/cm can be achieved. The discharge current risetime depends on the conductivity of the laser mixture and hence the preionization level. The 10% to 90% current risetime (as a function of time) is given by:

$$t_r(t) = \frac{2.2\ L}{R_d(t) + 2\ \Omega}$$

where L = 120 nh and R(t) is the total discharge resistance. For example with a constant discharge current density of 10^2 A/cm^2 and an electric field of 20 kV/cm, the discharge resistance is 10 Ω. Under these conditions a current risetime of 22 nsec would be achieved.

4. DIAGNOSTICS

Diagnostics for the measurement of e-beam and discharge voltages and currents, time-resolved and time-averaged fluorescence spectra and

discharge uniformity have all been developed. The gun cathode voltage is measured by means of an AERL-designed capacitive voltage probe located in the transition section between the gun spark gap and the gun cathode as shown in Figure 1. The total cathode current is also monitored in this transition section with a self-integrating Rogowski loop. A technique for measuring the total beam current transmitted to the discharge anode has also been developed. The laser cavity is first filled with ~ 25 Torr of SF_6. The discharge anode is then shorted to ground with a low inductance copper sheet. When the e-beam is fired, the beam current is forced to return through this sheet since the SF_6 scavenges the secondary electrons and prevents a plasma return current. The current which is monitored in this external ground return, after corrections for backscatter from the anode and gas and foil scattering, gives a measure of the beam current density in the laser cavity. The voltage across the discharge electrodes is measured in the manner described above. The discharge current is measured in the low inductance cathode ground return circuit as shown in Figure 3. Both 1/4 and 1/2 meter Jarrel-Ash monochrometers with photomultiplier tubes spanning a wide wavelength range in the visible and UV are available for time-resolved spectroscopy. Wavelength resolution to $\simeq 1$ Å is possible. Two Hilger prism spectrometers are also available for time-averaged spectroscopy. Finally, cameras for obtaining high resolution pictures of the discharge and its uniformity are also available.

II. ELECTRON-BEAM-CONTROLLED DISCHARGE PUMPING OF THE KrF LASER

Recently, lasing action in the rare-gas-monohalide systems has been predicted[1, 2] and observed.[3-5] To date these lasers have been pumped by high-energy e-beams only. In this chapter lasing action of KrF^* in an atmospheric-pressure electron-beam-controlled discharge is discussed.

Discharge pumping of these laser systems can lead ultimately to increased average laser power and efficiency over that achievable with e-beam pumping.[6] For e-beam pumping, the principal limitation on average laser power achievable can be calculated from the average power that can be put through the foil separating the electron gun vacuum chamber from the laser cavity. The limitations on the average power through this foil can be calculated from a consideration of the self-magnetic-field of the e-beam, foil heating, and beam energy. Pinching of the e-beam under the influence of its own magnetic field limits one dimension of the volume which can be pumped and therefore the single pulse energy (for a given beam energy and laser length). Foil heating limits the repetition rate at which the laser can operate. The repetition rate together with the single pulse energy

(1) J.J. Ewing and C.A. Brau, Phys. Rev. A12, 129 (1975).
(2) J.E. Velazco and D.W. Setser, J. Chem. Phys. 62, 1990 (1975).
(3) C.A. Brau and J.J. Ewing, Appl. Phys. Lett. 27, 435 (1975).
(4) J.J. Ewing and C.A. Brau, Appl. Phys. Lett. 27, 350 (1975).
(5) S.K. Searles and G.A. Hart, Appl. Phys. Lett. 27, 243 (1975).
(6) J.A. Mangano and J.H. Jacob (unpublished).

determines the average laser power. For fixed input power densities, e-beam-controlled discharge pumping requires e-beam current densities ≤ 0.2 of that required by pure e-beam pumping. Therefore, the limitations on average laser power discussed above are greatly reduced for a fixed pumping power density. This argument assumes, of course, comparable laser electrical efficiencies for both pumping methods. In fact, discharge pumping may be more efficient for the rare-gas-monohalide systems for three reasons:

(i) Beam energy losses in the foil and its support structure are less. (ii) Energy losses due to scattering of the electron beam in the foil and gas are reduced. (iii) Rare-gas metastable production efficiencies may be larger, 40-50% with e-beam pumping[7] against a possible 70% with discharge pumping.[8]

The laser experiments were carried out in the high-vacuum high-pressure discharge cavity that is described in detail in Section I. In the experiments, the beam from a cold cathode electron gun (150 keV, 8 A/cm^2, 300 nsec, 2 x 20 cm) was used to preionize atmospheric-pressure mixtures containing Ar, Kr, and F_2. The beam, which was generated in a vacuum chamber, entered the discharge cavity (2 x 2 x 20 cm^3) through an 80% transparent foil support structure, a 2-mil aluminized Kapton foil and a 70% transparent wire screen. The wire screen served as a grounded discharge

(7) R. M. Hill, R. A. Gutcheck, D. L. Huestis, D. Mukherjee, and D. C. Lorents, Stanford Research Institute Report No. MP74-39, 1974 (unpublished).

(8) In pure Ar, for example, the AERL Boltzmann code predicts a metastable production efficiency of 71% for electric fields of 2 kV/cm atm.

cathode. A stainless steel Rogowski-shaped discharge anode was placed 2 cm from this cathode. Approximately 40 nsec after the start of the e-beam pulse, a spark gap was triggered which switched a 0.3-μF capacitor across the discharge electrodes. A series 2-Ω water resistor was used to absorb most of the capacitor energy if arcing occurred, thereby preventing damage to the laser cavity.

Prior to filling, the discharge cavity was typically evacuated to $\leq 10^{-4}$ Torr with a LN_2-baffled diffusion pump system. The entire discharge cavity was passivated with a 1% F_2/99% Ar mixture for 2 h prior to the laser experiments. Gas mixtures were prepared in passivated stainless steel sample cylinders (1 liter) at pressures up to 10^3 psia and were allowed to stand for several hours before use to ensure complete mixing.

Optical access to the discharge cavity was provided by uv-grade quartz windows spaced 60 cm apart and aligned at Brewster's angle to the long (20 cm) dimension of the cavity. A stable 2.3-cm-diam optical resonator was formed by aligning flat and spherical (radius of curvature = 2 m) mirrors each having an output coupling of 1.3% at the KrF* laser wavelength. The mirrors were placed 80 cm apart.

In Table 1, the laser and discharge performance is summarized for six values of the mean discharge electric field. The input power by the e-beam was about 0.03 MW/cm^3. The laser mixture contained F_2/Kr/Ar at a total pressure of 1 atm. The mixture mole fractions were chosen to be 0.001/0.02/0.979, respectively, to minimize the formation of Kr dimers.[4] The first column in the table lists the observed total laser pulse energies as measured with a Scientech calorimeter (model 360203). From these data it can be seen that the laser pulse energy increases monotonically with increasing discharge electric field and therefore power input.

TABLE 1. LASER AND DISCHARGE PERFORMANCE FOR DIFFERENT VALUES OF THE DISCHARGE ELECTRIC FIELD

Laser Pulse Energy (mJ)	Pulse Width (nsec)	Onset Lag (nsec)	Efficiency (%)	Electric Field (kV/cm)	Mean Power Input (MW/cm^3)	Discharge Pulse Duration (nsec)
1.1	70	180	0.085	1.7	0.090	250
2.5	100	160	0.12	3.0	0.22	150
3.9	90	130	0.19	3.0	0.22	160
4.4	90	110	0.08	4.8	0.70	130
5.4	90	100	0.06	7.2	1.25	120
6.0	90	100	0.06	8.0	1.6	110

The laser electrical efficiency is defined here as the laser output energy divided by the discharge energy put into the laser cavity during the stable portion of the discharge pulse.[9] The measured laser efficiencies rise rapidly after laser threshold is reached, peak, and then decrease rapidly with increasing discharge power input. A possible explanation for the decrease in laser efficiency at higher input power is increased losses caused by metastable excitation and ionization as the metastable population becomes large. Energetic plasma electrons can, of course, readily excite and ionize the Kr and Ar metastables while 248.5-nm photons can ionize them.

The onset lag is defined as the time between discharge and laser turn on. As expected, this time lag is maximum near threshold and decreases to approximately 100 nsec with increasing pumping power. The magnitude of the onset lag is determined by the relevant kinetic transfer times and reaction rates as well as the discharge current risetime. Finally, the last column in Table 1 gives the duration of the stable portion of the discharge pulse before the onset of discharge arcing. At the larger electric field values, discharging arcing occurred simultaneously with e-beam turn off. Rapid e-beam turn off is accompanied by a large increase in plasma resistivity: F_2 attaches the discharge electrons. The subsequent increase in discharge voltage, induced by the circuit inductance and the rapid change in discharge current, results in immediate discharge arcing.

Laser and discharge performances were also investigated for six values of the laser mixture pressure between 0.75 and 3 atm. The F_2/Kr/Ar

(9) Obtaining the efficiency in this manner is valid because discharge experiments performed with no e-beam preionization of the atmospheric-pressure laser mixture resulted in immediate discharge arcing. No laser action was observed under these operating conditions.

mole fractions were held fixed at 0.001/0.02/0.979, respectively. The capacitor charge voltage in these experiments was 60 kV. It was found that laser action at 0.5 atm could not be achieved with discharge electric fields up to 5.6 kV/cm. For pressures $\geq$ 0.75 atm, laser action was achieved. The mean power input remained approximately constant at 1 MW/cm^3 and the input energy was about 0.1 J/cm^3 over the pressure range studied. The laser efficiency was found to vary between 0.05 and 0.08% and the laser output energy between 3.2 and 5.8 mJ. The onset lag and laser pulse width (FWHM) steadily decreased with increasing pressure: the former from 140 to 60 nsec and the latter from 90 to 40 nsec.

In Figure 4 oscillograms are presented which show the time variation of the electron gun cathode current, discharge voltage and current, and the laser pulse. These oscillograms were obtained under conditions similar to those described above. Note that the discharge voltage remains nearly constant for ~ 100 nsec and abruptly begins to decay. This discontinuity in discharge voltage slope marks the transition from a stable discharge to discharge arcing. A similar effect on total discharge current is also observed. The laser output pulse was attenuated by a factor of $\approx 10^4$ and viewed with a photodiode (ITT F4000 S5). Laser action was not observed with the mirror opposite the photodiode blocked. Peak laser powers in excess of 100 kW have been observed. However, in the laser experiments performed to date, the laser output always peaked after the termination of the stable portion of the discharge pumping pulse. Hence, no evidence of bottlenecking has been seen, indicating an unbound or very weakly bound lower laser level.[4] The spontaneous emission spectrum of KrF* is shown in Figure 5. This spectrum was obtained o:

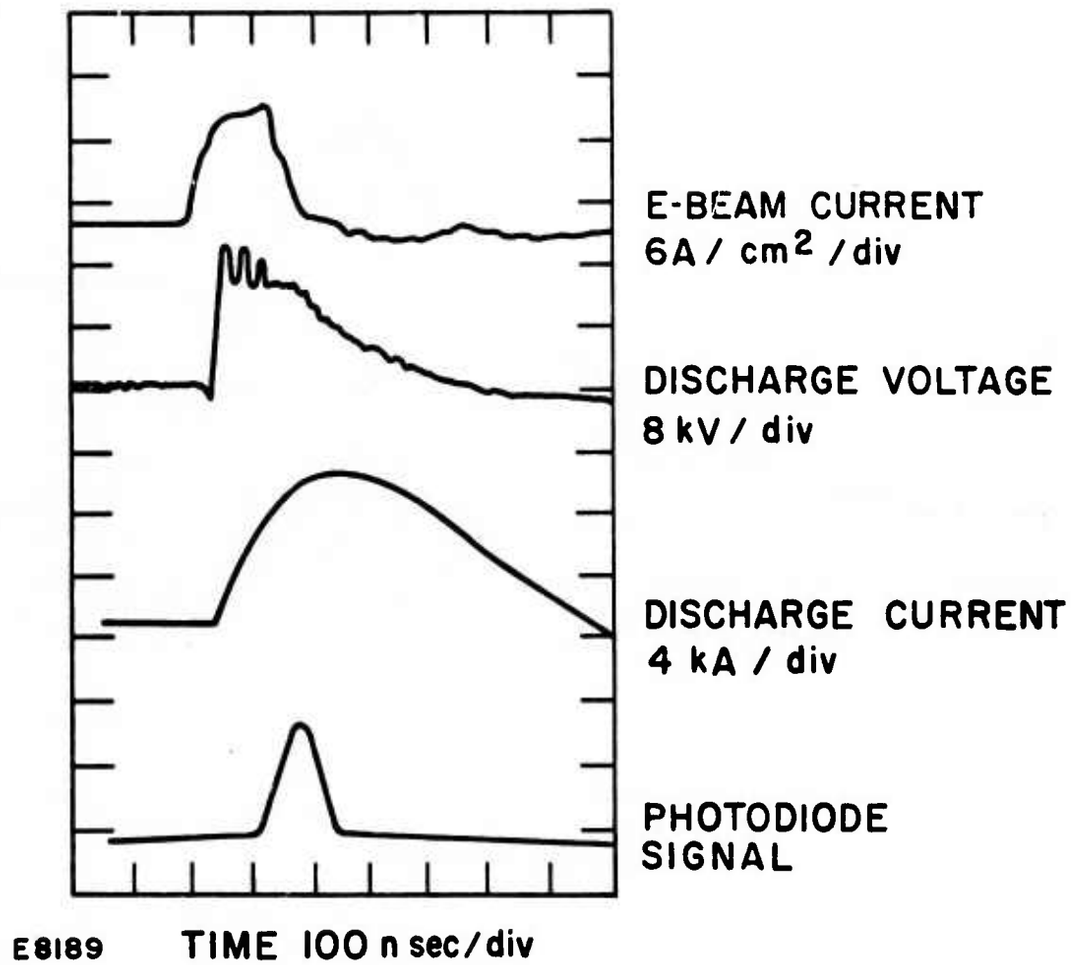

Figure 4 Oscillograms Showing Temporal Variation of E-beam Current, Discharge Voltage, Discharge Current and Laser Pulse

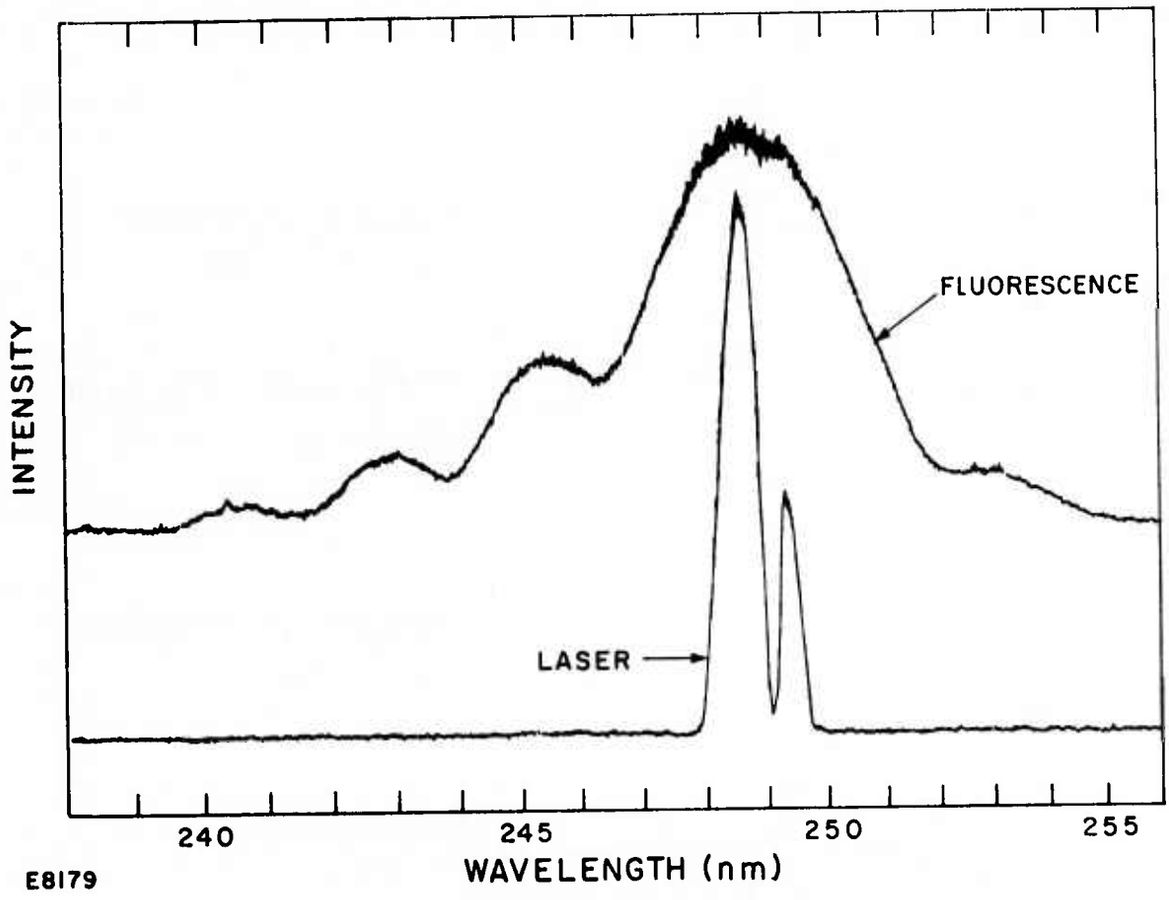

Figure 5 Spontaneous and Laser Spectra of KrF^*

a 1/2-m Hilger quartz spectrograph by removing one of the mirrors from the laser cavity and attenuating the spontaneous emission signal by a factor of 10. The vibrational band structure is clearly visible in the spectrum.[10] The lower trace shows the line narrowing characterizing laser action on these bands. Laser action is shown on two lines: the stronger at 248.5 nm and the weaker at 249.5 nm. The reason for the double line emission is presently not known.

Although the maximum efficiency observed in the discharge cavity was 0.2%, it is felt that much higher efficiencies are possible if most of the following cavity losses are eliminated: (i) Loss of 1.4% per pass per Brewster window. (ii) Loss of 2% per pass per atmosphere of the laser mixture through the 60 cm between windows because of F_2 absorption.[11] (iii) Loss of 0.4% per pass because of photoionization of Kr^*.[12] The output coupling was 1.3% per mirror. So the total loss per round trip was about 13% of which only 2.6% was output coupling. Therefore, the efficiency can probably be increased to about 1% by increasing the output coupling and eliminating the F_2 absorption regions at both ends of the cavity.

Threshold lasing by e-beam pumping alone was achieved in the laser cavity with an input power of 0.04 MW/cm^3. The total mixture pressure was 1.5 atm. From the considerations discussed above, the optical cavity loss was about 17%. Assuming that KrF* is produced by the following reaction:

---

(10) C.A. Brau and J.J. Ewing, J. Chem. Phys. (to be published).

(11) Jack G. Calvert and James N. Pitts, Jr., Photochemistry (Wiley, New York, 1966), p. 184.

(12) In computing the loss due to photoionization we have assumed a cross section of 10^{-19} cm^2. This is just the photoionization cross section of Rb at 2485 Å.

$$Kr^* + F_2 = KrF^* + F$$

and the lifetime of KrF^* is 10 or 20 nsec, a branching ratio of 0.15 - 0.3 is estimated. The branching ratio is < 1 because $Kr^* + F_2$ can form other products. If Kr^* can be produced with a 75% efficiency in a discharge, the possible efficiency of the KrF laser is 5-10%.

III. N_2/NO LASER KINETICS

1. INTRODUCTION

In this section we investigate the possibility of making an NO γ-band laser by energy transfer from $N_2(A)$. The A-state of N_2 transfers its energy efficiently and rapidly to NO(A) which subsequently radiates on several bands. The most intense bands are between 236-285 nm. From a linear Boltzmann code analysis the results of which are shown in Figure 6, it appears that at electric fields of 24 kV/cm-atm 30-40% of the energy ends up in the electronic states of nitrogen. Most of this energy will cascade to the A-state.

Figure 7 shows typical N_2/NO discharge data. The mixture contained 3 Torr of NO in an atmosphere of N_2. For the run shown in Figure 7 the electric field obtained for the first 150 ns was slightly greater than 25 kV/cm atm. The mean discharge current at this electric field was about 100 A/cm^2 and the energy deposited in the gas was 375 J/liter. The initial voltage drop is due to the capacitor discharging. An arc occurred about 500 ns after the discharge voltage was applied. This indicates that we could put in an even greater amount of energy at these voltages. In Figure 7 we also see the fluorescence at 2362 Å corresponding to the NO(A, v = 0) → NO(X, v = 1) transition. The fluorescence increased when the voltage is turned on and begins to decay as the discharge voltage decreases. The second increase in the signal is noise from the arc. Notice that the time scales in the upper and lower photographs are 100 ns/div. and 200 ns/div. respectively.

In Figure 8 we see a time-averaged spectrum of the light from the N_2/NO discharge. It is apparent from this figure that <u>most</u> of the radiated

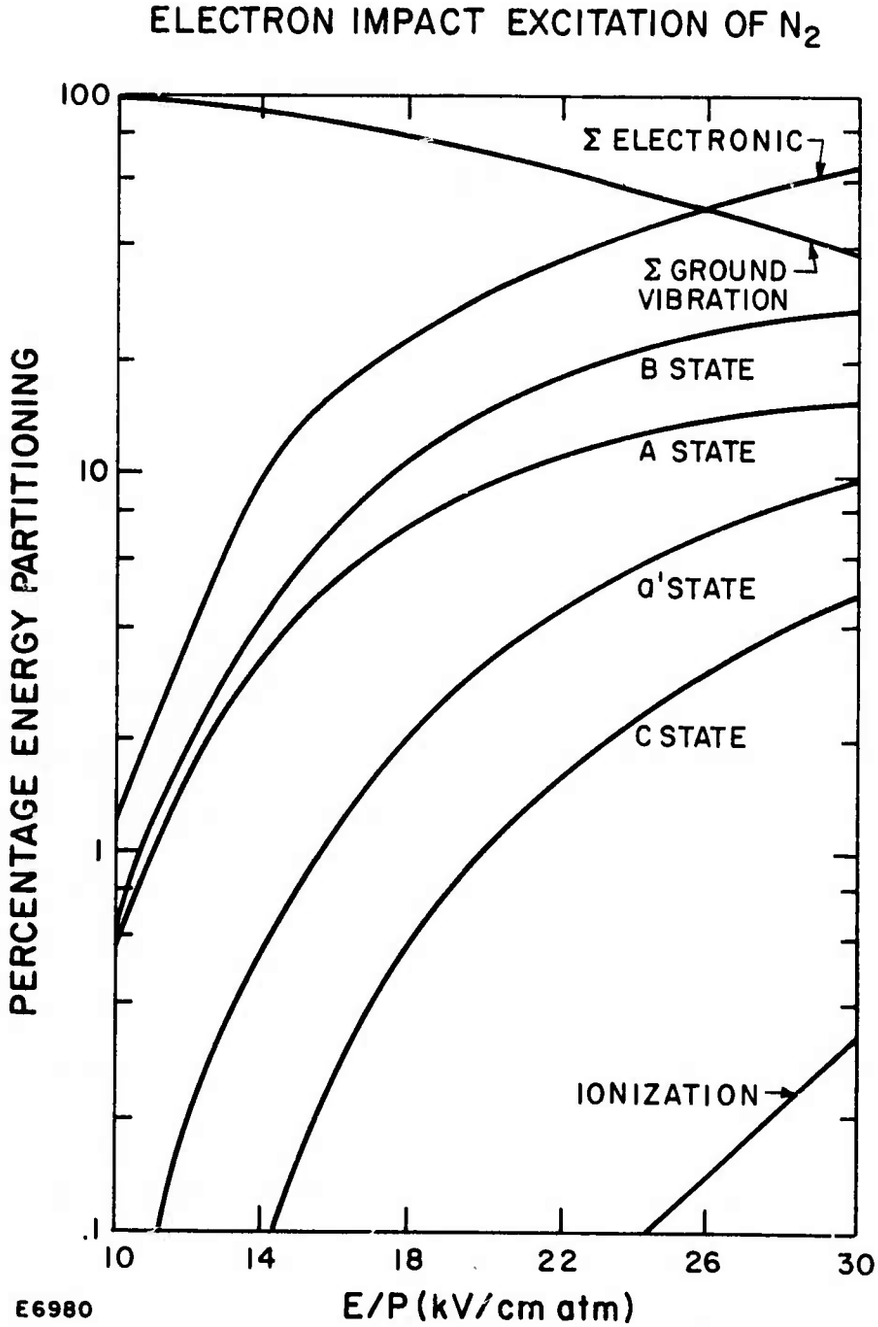

Figure 6 Fraction of Discharge Energy into Various Excited States of N_2 as a Function of E/p as Predicted by the Boltzmann Code

N_2/NO DISCHARGE

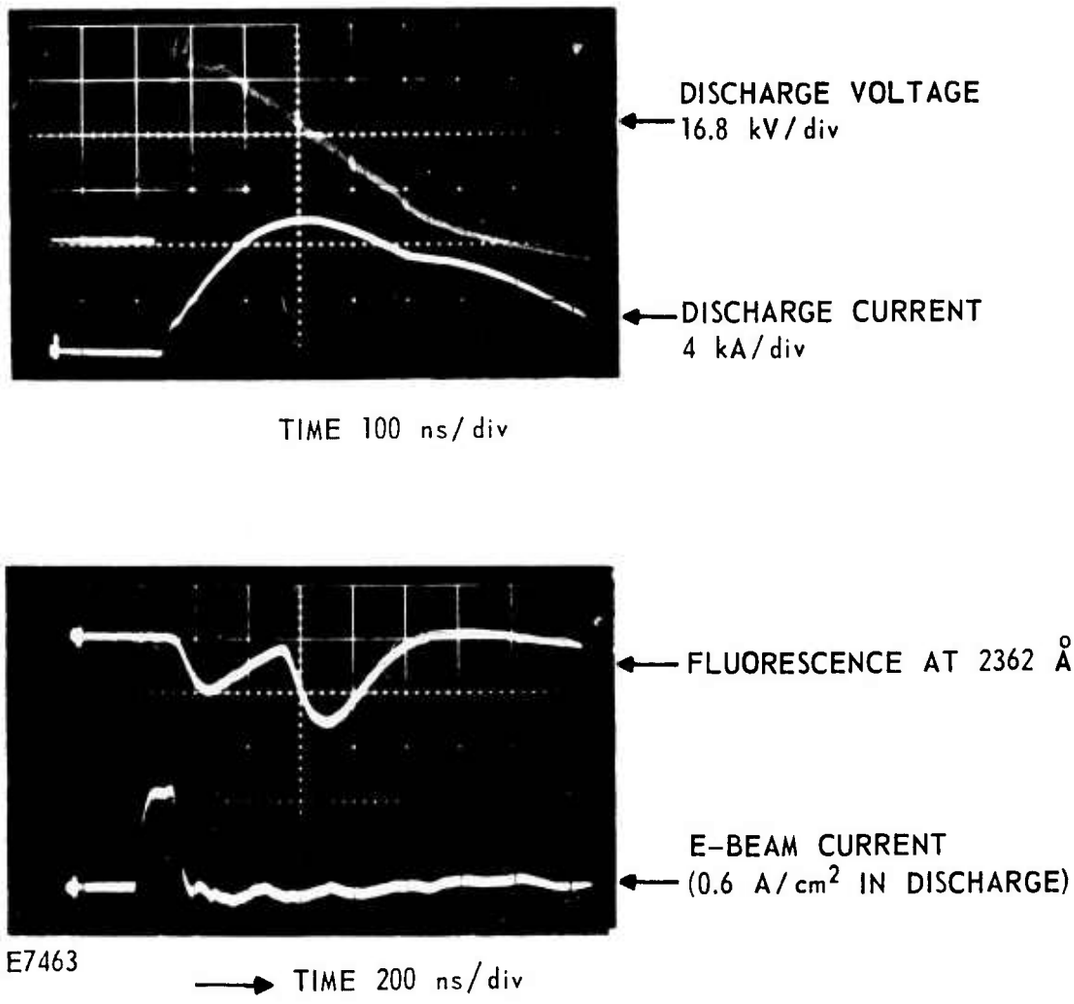

Figure 7 Experimental Results in N_2/NO Discharge

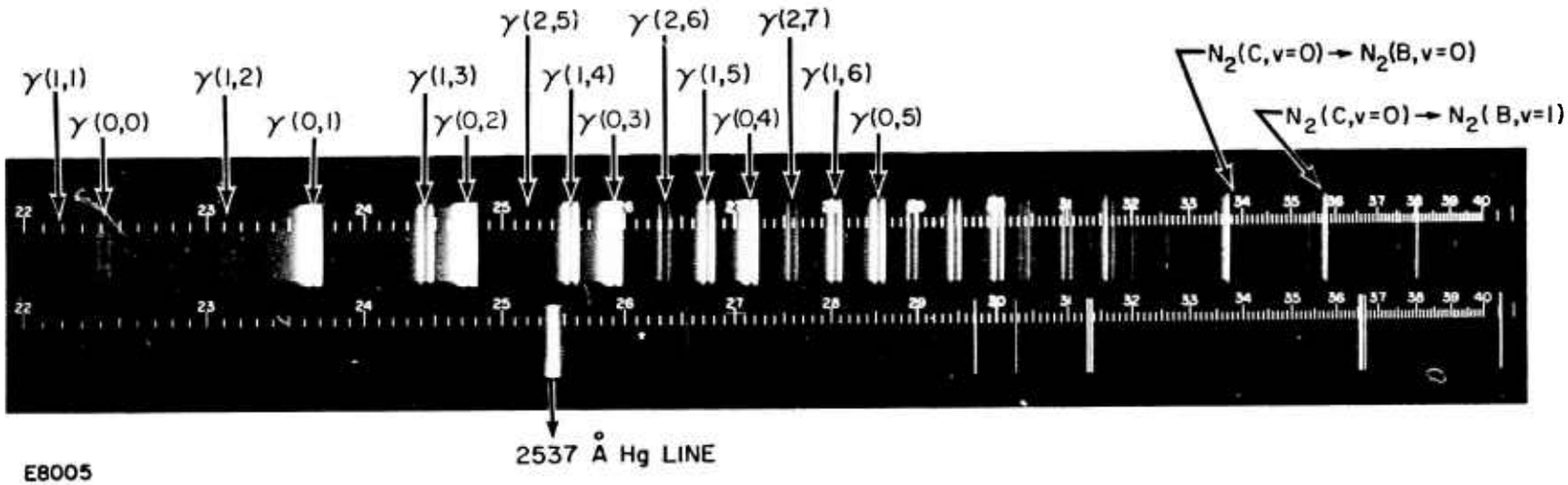

Figure 8 Time Averaged Spectrum of Light from an N_2/NO Discharge. Partial pressure of NC was 3 torr in an atmosphere of N_2. Also shown in a Hg spectrum.

energy emanates in the γ-bands of NO indicating efficient transfer from $N_2(A)$ to NO(A). The NO(A, v = 0) → NO(X, v = 0) is faint because the photographic plate is extremely insensitive below 2300 Å. Also shown in Figure 8 for the purpose of precise wavelength calibration, is a mercury spectrum. Because of these results we investigated the possibility of obtaining lasing action on the NO γ-bands. Unfortunately because of the lack of time the research was limited to theory only.

2. $N_2(A)$ PRODUCTION IN A DISCHARGE

From Figure 6 it is clear that the discharge energy is split into primarily the A and B states of N_2. Some of the energy is also depicted into the a' and C states. Unfortunately very little is known about the kinetics of the a' state and so we will ignore it in the subsequent discussion. The rate equations for $N_2(A)$, $N_2(B)$ and $N_2(C)$ are:

$$\frac{dN_2(A)}{dt} = \frac{R_A \dot{\Theta}_E}{KT_A} + N_2\, k_{BA}\, N_2(B) + \frac{N_2(B)}{\tau_B} - k_p \left\{N_2(A)\right\}^2 \qquad (1)$$

$$\frac{dN_2(B)}{dt} = \frac{R_B \dot{\Theta}_E}{KT_B} + N_2\, k_{BC}\, N_2(C) + \frac{N_2(C)}{\tau_C} + 0.8\, k_p \left\{N_2(A)\right\}^2 - \frac{N_2(B)}{\tau_B} - N_2\, k_{BA}\, N_2(B) \qquad (2)$$

$$\frac{dN_2(C)}{dt} = \frac{R_C \dot{\Theta}_E}{KT_C} + 0.2\, k_p \left\{N_2(A)\right\}^2 - \frac{N_2(C)}{\tau_C} - N_2\, k_{BC}\, N_2(C) \qquad (3)$$

where R_A, R_B and R_C is the fraction of discharge energy going into the A, B and C states, respectively. K is the Boltzmann constant and T_A, T_B and T_C is the energy of the A, B and C states. k_{BA} and k_{BC} are the deactivation rates of $N_2(B) \rightarrow N_2(A)$ and $N_2(C) \rightarrow N_2(B)$ while k_p is the $N_2(A)$ pooling

reaction. Detailed kinetics done by SRI show that about 80% of the pooling reaction form $N_2(B)$ while 20% eventually forms $N_2(C)$. $\dot{\Theta}_E$ is the discharge power input per unit volume. The simultaneous solution of Eqs. (1) - (3) will give the temporal populations of $N_2(A)$, $N_2(B)$ and $N_2(C)$. However, if we are interested in only the $N_2(A)$ state and time resolution of $\geq$ 20 ns, we can reduce the three equations to one.

At an atmosphere the deactivation time of $N_2(C)$ by nitrogen is about 3 ns, while $N_2(B)$ is deactivated in 20 nsec. So if we are not interested in time scales of 20 ns and less, the rate equation for $N_2(A)$ becomes

$$\frac{dN_2(A)}{dt} = \frac{R_T \dot{\Theta}_E}{KT_A} - \frac{1}{2} k_p \left\{N_2(A)\right\}^2 \tag{4}$$

where

$$R_T = \left(\frac{R_A}{KT_A} + \frac{R_B}{KT_B} + \frac{R_C}{KT_B}\right) KT_A$$

The pooling rate as measured by SRI is 10^{-10} cm^3/sec. The factor 1/2 in Eq. (4) is to account for return to $N_2(A)$ from $N_2(B)$ or $N_2(C)$. Equation (4) can be integrated to give (assuming $\dot{\Theta}_E$ is constant)

$$N_2(A) = \sqrt{\frac{2R_T \dot{\Theta}_E}{k_p}} \; \frac{e^{t/\tau} - 1}{e^{t/\tau} + 1} \tag{5}$$

where

$$\tau = \frac{1}{\sqrt{2 k_p R_T \dot{\Theta}_E / KT_A}} \tag{6}$$

As an example, let's consider the peak $N_2(A)$ density for discharge parameters achieved in our experiment to date. We have deposited 375 J/liter in 150 ns at electric fields in excess of 25 kV/cm-atm. So $\dot{\Theta}_E$ is

2.5×10^6 watt/cc. From Figure 6, $R_T \approx 0.3$. Substituting into Eq. (6), we find that $\tau = 8.1 \times 10^{-8}$ sec. So after 150 ns, the $N_2(A)$ density is approximately $8.5 \times 10^{16}/cm^3$.

3. N_2/NO DISCHARGE KINETICS

If we add 3 torr or less of NO to an atmosphere of N_2 then we have to account for the deactivation of $N_2(A)$, $N_2(B)$ and $N_2(C)$ by NO. These deactivation rates have been measured recently by SRI. Once again, however, we can reduce the three rate equations to a single equation if we are interested in times of 20 ns and longer. Equation (4) can then be rewritten as

$$\frac{dN_2(A)}{dt} = R_T \dot{\theta}_E - \frac{k_p}{2} \left\{N_2(A)\right\}^2 - k_{OA}\, N_2(A)\, NO \tag{7}$$

where k_{OA} ($\approx 8 \times 10^{-11}$ cm^3/sec) is the rate at which $N_2(A)$ is deactivated by NO. In writing Eq. (7) we have also assumed that $N_2(B)$ and $N_2(C)$ are deactivated by N_2 only. This assumption is valid provided that the fraction of NO present in the N_2-NO mix is $\leq 10^{-2}$.

Equation (7) can be integrated to give for times $\leq t_p$ the pulse time to give

$$N_2(A) = \frac{N_o \tanh(\epsilon t)\left[\left(\frac{k_p N_o}{2}\right) + \beta\right](\exp 2\epsilon t + 1)}{\left\{\left(\frac{k_p}{2} N_o + \beta\right)(\exp(2\epsilon t) + 1) - \beta\right\}} \tag{8}$$

where

$$N_o = \frac{1}{2}\left\{\left[\left(\frac{2\beta}{k_p}\right)^2 + \frac{8R_T\dot{\theta}_E}{kT_A k_p}\right]^{1/2} - \frac{2\beta}{k_p}\right\} \tag{9}$$

and

$$\epsilon = \frac{k_p N_o}{2} + \frac{\beta}{2} \tag{10}$$

We can now approximately compute the NO(A) number density by integrating the following equation

$$\frac{d}{dt}\,NO(A) = \frac{k_{OA}}{2}\,N_2(A)\,NO - NO(A)\left[\frac{1}{\tau_A} = k_{ON}\,NO\right] \tag{11}$$

where τ_A is the spontaneous radiative lifetime of NO and k_{ON} is the deactivation rate of NO(A) by NO. Integrating Eq. (11) we find

$$NO(A) = \frac{k_{OA}}{2}\,NO\,\exp(t/\tau)\int_0^t dt_1\,N_2(A)\,\exp(-t_1/\tau) \tag{12}$$

where

$$\frac{1}{\tau} = \left(\frac{1}{\tau_A} + k_{ON}\,NO\right) \tag{13}$$

The reason that we divide the first term on the RHS of Eq. (11) by 2 is because, according to SRI, only 50% of $N_2(A)$ deactivation goes into making NO(A).

In Figures 9, 10, and 11 we see the results of having 10^{15}, 10^{16} and $10^{17}/cm^3$ of NO in a square-topped pulse of 200 ns duration. The conditions are similar to the discharge conditions obtained in our experiment except Θ_E in our discharge was not square-topped. Notice that the peak NO(A) population increases from 2×10^{14} to $6 \times 10^{15}/cm^2$. For the conditions run in our discharge we expect about 25% less energy into the $N_2(A)$. As a result for an NO concentration of $10^{17}/cm^3$ we expect an NO(A) density of about $4 \times 10^{15}/cm^3$.

4. GAIN OF NO γ-BANDS

The gain G between an NO(A) vibrational level v' and a ground state vibrational level v'' is given by

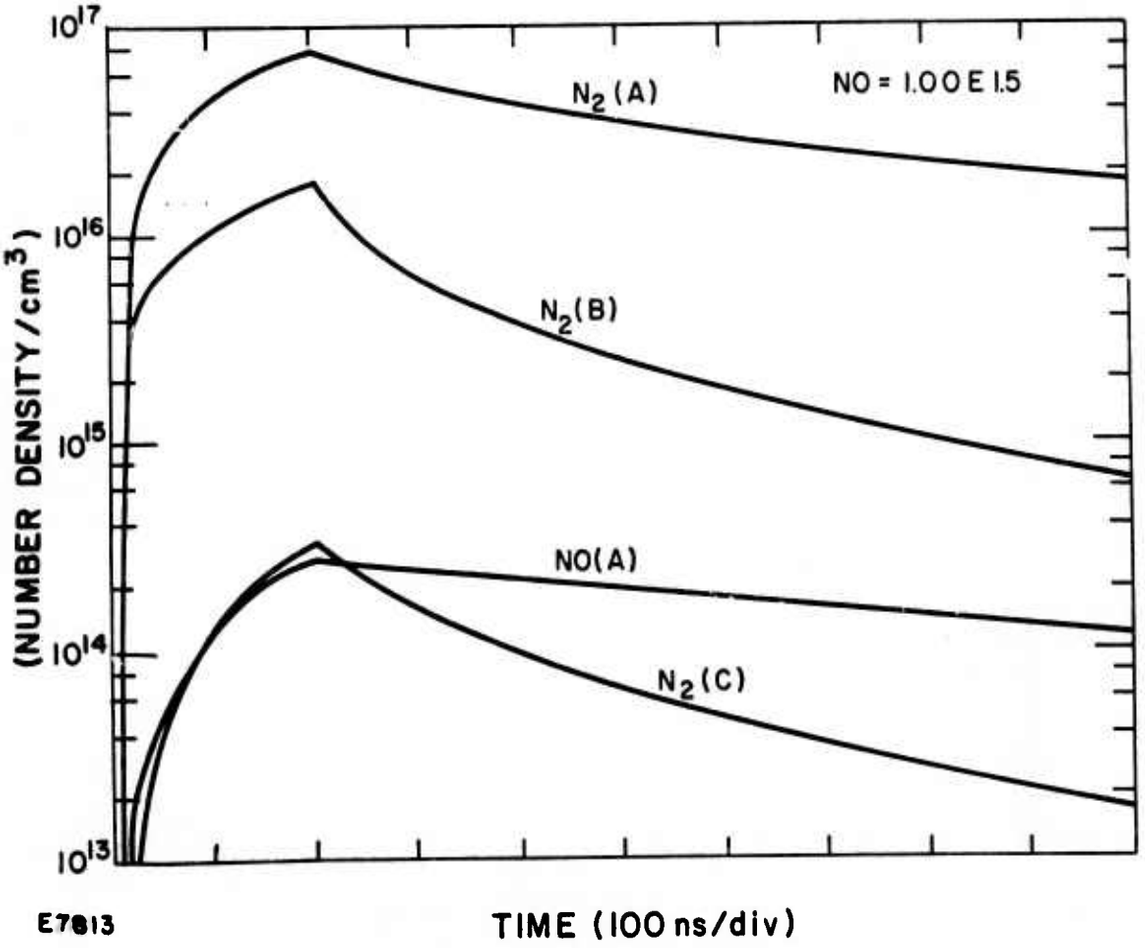

Figure 9 Predicted Temporal Evolution of the $N_2(A)$, $N_2(B)$, $N_2(C)$ and NO(A) States. The electrical power input is assumed to be square topped and 200 ns in length. The NO number density is $10^{15}/cm^3$.

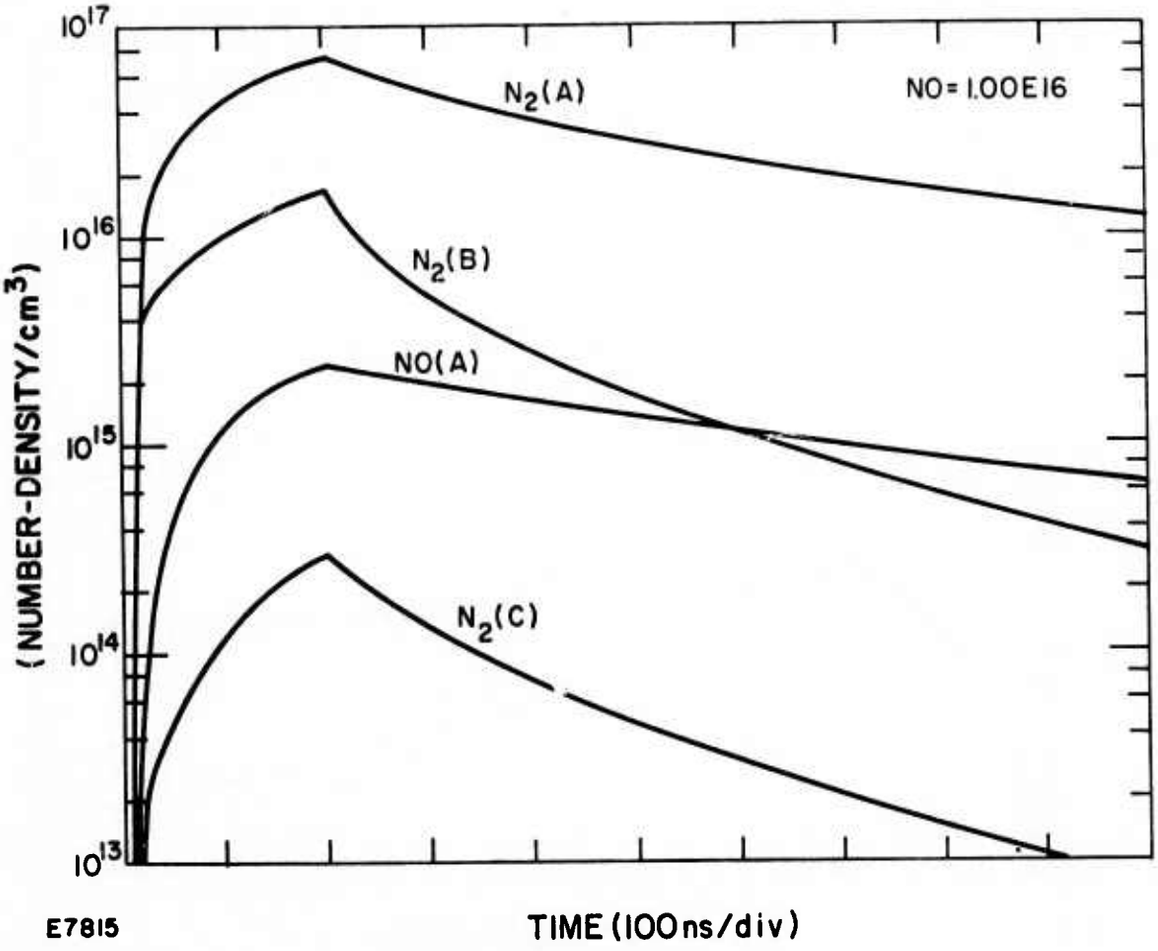

Figure 10 Predicted Temporal Evolution of the $N_2(A)$, $N_2(B)$, $N_2(C)$ and NO(A) States. The electrical power input is assumed to be square topped and 200 ns in length. The NO number density is $10^{16}/cm^3$.

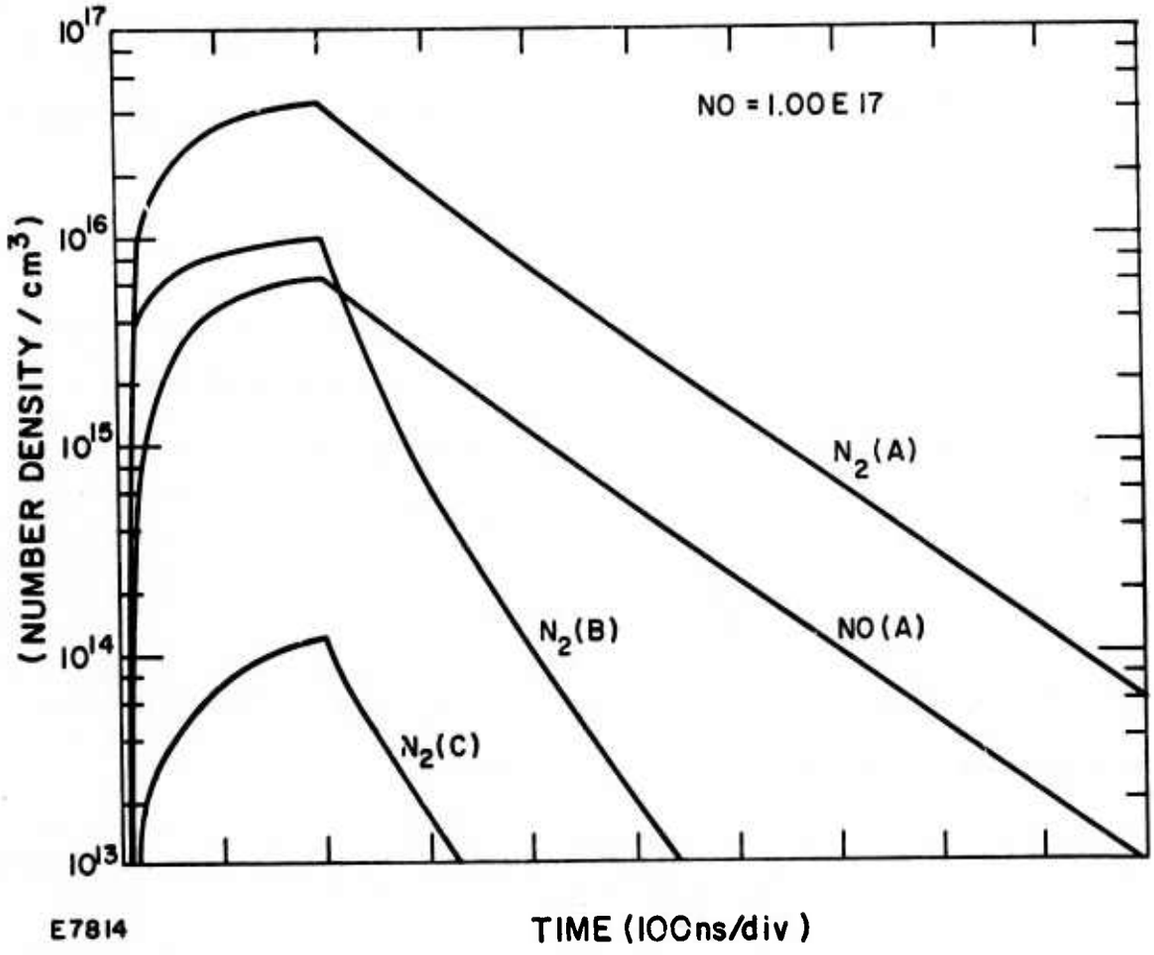

Figure 11 Predicted Temporal Evolution of the $N_2(A)$, $N_2(B)$, $N_2(C)$ and NO(A) States. The electrical power input is assumed to be square topped and 200 ns in length. The NO number density is $1017/cm^3$.

$$G(v', v'') = \frac{\lambda^2}{8\pi\Delta\nu} \frac{1}{\tau(v', v'')} \frac{N_{v'}(J)}{g} \tag{14}$$

where τ is the spontaneous lifetime, g is the degeneracy factor, λ the wavelength, $\Delta\nu$ the line width and $N_{v'}(J)$ the inversion density of a particular rotational line J

$$N_{v'}(J) = \frac{N_{v'}(2J+1)}{KT/B} \exp\left[\frac{-BJ(J+1)}{KT}\right] \tag{15}$$

where $N_{v'}$ is total number density of the NO(A)v' level. We are assuming that the lower level has a negligible population. This assumption has been investigated thoroughly and will be discussed subsequently. For NO(A) $B/K = 2.8^{o}K$ and the peak population occurs at J_m where

$$J_m = \sqrt{\frac{KT}{2B}} - \frac{1}{2} \approx 6.7 \text{ i.e., } 7 \tag{16}$$

The spontaneous lifetime $\tau(v', v'')$ can be computed from the oscillator strengths f using the following expression

$$f\tau = \frac{mc}{8\pi e^2} \lambda^2 = 1.51 \lambda^2 \tag{17}$$

and

$$f(v', v'') = \frac{8\pi^2 mc}{3he^2} \nu(v', v'') \overline{R}_e^{\,2} q(v', v'') \tag{18}$$

where $q(v', v'')$ is the Franck-Condon factor. Because R_e is slowly varying we will assume it is a strict constant. f(0, 0) has been measured experimentally[13] to be

$$f(0, 0) = 3.9 \times 10^{-4} \text{ sec}^{-1}$$

(13) G. W. Bethke, J. Chem. Phys. 31, 662 (1959).

From Eq. (18) we can write

$$f(0, v'') = \frac{f(0, 0)}{q(0, 0)} \frac{\nu(0, v'')}{\nu(0, 0)} q(0, v'') \tag{19}$$

The Franck-Condon factors have been computed in great detail[14] so we can now write Eq. (14) as

$$G(0, v'') = \frac{1}{106\pi} \frac{0.083 N_v}{\Delta\nu} \frac{f(0, v'')}{1.51} \tag{20}$$

In arriving at Eq. (20) we have assumed a degeneracy factor of 12. In particular the gain of the most promising bands is

$$\begin{aligned} G(0, 1) &= 2.7 \times 10^{-17} N_o/\text{cm} \\ G(0, 2) &= 2.3 \times 10^{-17} N_o/\text{cm} \\ G(0, 3) &= 1.5 \times 10^{-17} N_o/\text{cm} \\ G(0, 4) &= 8.1 \times 10^{-18} N_o/\text{cm} \\ G(0, 5) &= 3.9 \times 10^{-18} N_o/\text{cm} \end{aligned} \tag{21}$$

So for the peak predicted NO(A) population of 4×10^{15} cm^{-3} the maximum gain is only about 10%/cm. For such a gain, and no active medium absorption, lasing should be possible in our present cavity.

5. POPULATION OF THE GROUND VIBRATIONAL LEVELS OF NO

The NO ground vibrational levels are the lower laser levels and hence it is of interest to investigate the rate at which they are produced in a discharge. There are three primary methods by which they can be produced: (1) direct electron impact; and (2) transfer from N_2 ground vibrational levels; and (3) $N_2(A)$ deactivation by NO. We will discuss each method separately.

(14) H. P. Broida and H. M. Poland, Bull. Am. Phys. Soc. 15, 1526 (1970).

(a) Direct Electron Impact

Spence and Shulz[15] have recently measured the electron impact cross section for pumping NO ground vibrational levels and found that each had a series of sharp peaks having a maximum amplitude of 10^{-17} cm^2 and a half-width of 0.05 eV. We have put these cross sections into our Boltzmann code and obtained a predicted pumping rate of about 4×10^{-11} cm^3/sec. So in the presence of 2 torr of NO and a discharge current of 100 A/cm^2 the rate of producing ground-state vibrational levels is about 3×10^{19} sec^{-1}. The rate for producing NO(A) is 10^{22} - 10^{23}/sec. So we see that NO(A) is produced at a rate that is two to three orders of magnitude faster than by electron impact, so we can neglect electron impact excitation of the NO ground levels.

(b) Transfer from N_2 Vibrational Levels

The transfer from $N_2(v = 1)$ to $NO(v = 1)$ has been measured[16] and found to be 1.2×10^{-15} cm^3/sec. If we assume that $N_2(v = 1)$ is deactivated at a negligible rate we can write

$$N_2(v = 1) = k_1 \, n_e \, N_2 \, t \tag{22}$$

where k_1 is the rate of producing $N_2(v = 1)$ in a discharge. n_e is the electron density, N_2 is the nitrogen number density and t the time. Further, if we neglect the loss rate of $NO(v = 1)$ we can write

$$NO(v = 1) = 6 \times 10^{-16} \, k_1 \, n_e \, N_2 \, NO \, t^2 \tag{23}$$

k_1 has been evaluated by the Boltzmann code to be 1.85×10^{-9}. A discharge current density of 100 A/cm^2 corresponds to $n_e \approx 5 \times 10^{13}/cm^3$. So after 200 ns population of $NO(v = 1)$ is about $6 \times 10^{12}/cm^3$ and hence is negligible.

(15) Spence and Shulz, Phys. Rev. A3, 1968 (1971).

(16) P.F. Lewis and D.W. Trainor, Avco Everett Research Laboratory, AMP 422 (1974).

The vibrational levels of NO(X) can also be pumped by the $N_2(X)$ vibrational levels in the following manner

$$N_2(v = n) + NO(v = 0) = NO(v = 1) + N_2(v = n - 1)$$

Unfortunately these rates haven't been measured. Because of the anharmonicity this rate will increase with increasing n. However, this increase will probably be partially offset by the decrease of the vibrational population with increasing n. Estimates based on the rates predicted by the Boltzmann code and anharmonicity of the N_2 vibrational levels give a population for $NO(X, v = 1) \approx 6 \times 10^{13}/cm^3$ after 200 ns. This population is 10-100 times smaller than the predicted NO(A) number density and hence negligible.

(c) $N_2(A)$ Deactivation by NO(X)

SRI have made careful measurements of the deactivation of $N_2(A)$ by NO(X). They have concluded that about 50% of the energy goes into NO(A) and 25% into NO(B). They haven't accounted for the remaining 25%. If this energy goes directly to one lower vibrational level of NO(X), it could be significant. However, because of the big energy difference and the number of vibrational levels, it appears unlikely that there will be appreciable pumping of NO(X) by $N_2(A)$.

IV. REFERENCES

1. J.J. Ewing and C.A. Brau, Phys. Rev. A12, 129 (1975).

2. J.E. Velazco and D.W. Setser, J. Chem. Phys. 62, 1990 (1975).

3. C.A. Brau and J.J. Ewing, Appl. Phys. Lett. 27, 435 (1975).

4. J.J. Ewing and C.A. Brau, Appl. Phys. Lett. 27, 350 (1975).

5. S.K. Searles and G.A. Hart, Appl. Phys. Lett. 27, 243 (1975).

6. J.A. Mangano and J.H. Jacob (unpublished).

7. R.M. Hill, R.A. Gutcheck, D.L. Huestis, D. Mukherjee, and D.C. Lorents, Stanford Research Institute Report No. MP74-39, 1974 (unpublished).

8. In pure Ar, for example, the AERL Boltzmann code predicts a metastable production efficiency of 71% for electric fields of 2 kV/cm atm.

9. Obtaining the efficiency in this manner is valid because discharge experiments performed with no e-beam preionization of the atmospheric-pressure laser mixture resulted in immediate discharge arcing. No laser action was observed under these operating conditions.

10. C.A. Brau and J.J. Ewing, J. Chem. Phys. (to be published).

11. Jack G. Calvert and James N. Pitts, Jr., Photochemistry (Wiley, New York, 1966), p. 184.

12. In computing the loss due to photoionization we have assumed a cross section of 10^{-19} cm^2. This is just the photoionization cross section of Rb at 2485 Å.

13. G.W. Bethke, J. Chem. Phys. 31, 662 (1959).

14. H.P. Broida and H.M. Poland, Bull. Am. Phys. Soc. 15, 1526 (1970).

15. Spence and Shulz, Phys. Rev. A3, 1968 (1971).

16. P.F. Lewis and D.W. Trainor, Avco Everett Research Laboratory, AMP 422 (1974).

DISTRIBUTION LIST

Office of Naval Research, Department of the Navy, Arlington, VA 22217 - Attn: Physics Program (3 copies)

Naval Research Laboratory, Department of the Navy, Washington, D.C. 20375 - Attn: Technical Library (1 copy)

Office of the Director of Defense, Research and Engineering, Information Office Library Branch, The Pentagon, Washington, D.C. 20301 (1 copy)

U.S. Army Research Office, Box CM, Duke Station, Durham, N.C. 27706 (1 copy)

Defense Documentation Center, Cameron Station, Alexandria, VA 22314 (12 copies)

Defender Information Analysis Center, Battelle Memorial Institute, 505 King Avenue, Columbus, OH 43201 (1 copy)

Commanding Officer, Office of Naval Research Branch Office, 536 South Clark Street, Chicago, IL 60615 (1 copy)

New York Area Office, Office of Naval Research, 715 Broadway (5th Floor), New York, NY 10003 - Attn: Dr. Irving Rowe (1 copy)

San Francisco Area Office, Office of Naval Research, 760 Market Street, Room 447, San Francisco, CA 94102 (1 copy)

Air Force Office of Scientific Research, Department of the Air Force, Washington, D.C. 22209 (1 copy)

Office of Naval Research Branch Office, 1030 East Green Street, Pasadena, CA 91106 - Attn: Dr. Robert Behringer (1 copy)

Code 102 1P (ONRL), Office of Naval Research, 800 N. Quincy Street, Arlington, VA 22217 (6 copies)

Defense Advanced Research Projects Agency, 1400 Wilson Blvd., Arlington, VA 22209 - Attn: Strategic Technology Office (1 copy)

Office Director of Defense, Research & Engineering, The Pentagon, Washington, D.C. 20301 - Attn: Assistant Director (Space and Advanced Systems) (1 copy)

Office of the Assistant Secretary of Defense, System Analysis (Strategic Programs), Washington, D.C. 20301 - Attn: Mr. Gerald R. McMichels (1 copy)

U.S. Arms Control and Disarmament Agency, Dept. of State Bldg., Rm. 4931, Washington, D.C. 20451 - Attn: Dr. Charles Henkin (1 copy)

Energy Research Development Agency, Division of Military Applications, Washington, D.C. 20545 (1 copy)

National Aeronautics and Space Administration, Lewis Research Center, Cleveland, OH 44135 - Attn: Dr. John W. [illegible], Jr. (1 copy)
(Aerospace Res. Engineer)

National Aeronautics & Soace Administration, Code RR, FOB 10B, 600 Independence Ave., SW, Washington, D.C. 20546 (1 copy)

National Aeronautics and Space Administration, Ames Research Center, Moffett Field, CA 94035 - Attn: Dr. Kenneth W. Billman (1 copy)

Department of the Army, Office of the Chief of RD&A, Washington, D.C. 20310 - Attn: DARD-DD (1 copy)
DAMA-WSM-T (1 copy)

Department of the Army, Office of the Deputy Chief of Staff for Operations & Plans, Washington, D.C. 20310 - Attn: DAMO-RQD - (1 copy)

Ballistic Missile Defense Program Office (BMDPO), The Commonwealth Building, 1300 Wilson Blvd., Arlington, VA 22209 - Attn: Mr. Albert J. Bast, Jr. (1 copy)

U.S. Army Missile Command, Research & Development Division, Redstone Arsenal, AL 35809 - Attn: Army High Energy Laser Programs (2 copies)

Commander, Rock Island Arsenal, Rock Island, IL 61201, Attn: SARRI-LR, Mr. J.W. McGarvey (1 copy)

Commanding Officer, U.S. Army Mobility Equipment R&D Center, Ft. Belvoir, VA 22060 - Attn: SMEFB-MW (1 copy)

Commander, U.S. Army Armament Command, Rock Island, IL 61201 - Attn: AMSAR-RDT (1 copy)

Director, Ballistic Missile Defense Advanced Technology Center, P.O. Box 1500, Huntsville AL 35807 - Attn: ATC-O (1 copy)
ACT-T (1 copy)

Commander, U.S. Army Material Command, Alexandria, VA 22304 - Attn: Mr. Paul Chernoff (AMCRD-T) (1 copy)

Commanding General, U.S. Army Munitions Command, Dover, NH 17801 - Attn: Mr. Gilbert F. Chesnov (AMSMU-R) (1 copy)

Director, U.S. Army Ballistics Res. Lab, Aberdeen Proving Ground, MD 21005 - Attn: Dr. Robert Eichenberger (1 copy)

Commandant, U.S. Army, Air Defense School, Ft. Bliss, TX 79916 - Attn: Air Defense Agency (1 copy)
ATSA-CTD-MS (1 copy)

Commanding General, U.S. Army Combat Dev. Command, Ft. Belvoir, VA 22060 - Attn: Director of Material, Missile Div. (1 copy)

Commander, U.S. Army Training & Doctrine Command, Ft. Monroe, VA 23651 - Attn: ATCD-CF (1 copy)

Commander, U.S. Army Frankford Arsenal, Philadelphia, PA 19137 - Attn: Mr. M. Elnick SARFA-FCD Bldg. 201-3 (1 copy)

Commander, U.S. Army Electronics Command, Ft. Monmouth, NJ 07703 - Attn: AMSEL-CT-L, Dr. R.G. Buser (1 copy)

Commander, U.S. Army Combined Arms Combat Developments Activity, Ft. Leavenworth, KS 66027 (1 copy)

National Security Agency, Ft. Geo. G. Meade, MD 20755 - Attn: R.C. Foss A763 (1 copy)

Deputy Commandant for Combat & Training Developments, U.S. Army Ordnance Center and School, Aberdeen Proving Ground, MD 21005
Attn: ATSL-CTD-MS-R (1 copy)

Commanding Officer, USACDC CBR Agency, Ft. McClellan, AL 36201 - Attn: CDCCBR-MR (Mr. F.D. Poer) (1 copy)

DISTRIBUTION LIST (Continued)

Department of the Navy, Office of the Chief of Naval Operations, The Pentagon 5C739, Washington, D.C. 20350 - Attn: (OP 982F3) (1 copy)

Office of Naval Research Branch Office, 495 Summer Street, Boston, MA 02210 - Attn: Dr. Fred Quelle (1 copy)

Department of the Navy, Deputy Chief of Navy Material (Dev.), Washington, D.C. 20360 - Attn: Mr. R. Gaylord (MAT 0321B) (1 copy)

Naval Missile Center, Point Mugu, CA 93042 - Attn: Gary Gibbs (Code 5352) (1 copy)

Naval Research Laboratory, Washington, D.C. 20375 - Attn: (Code 5503-EOTPO) (1 copy)
Dr. P. Livingston - Code 5560 (1 copy)
Dr. A. I. Schindler - Code 6000 (1 copy)
Dr. H. Shenker - Code 5504 (1 copy)
Mr. D. J. McLaughlin - Code 5560 (1 copy)
Dr. John L. Walsh - Code 5503 (1 copy)

High Energy Laser Project Office, Department of the Navy, Naval Sea Systems Command, Washington, D.C. 20360 - Attn: Capt. A. Skolnick, USN (PM 22) (1 copy)

Superintendent, Naval Postgraduate School, Monterey, CA 93940 - Attn: Library (Code 2124) (1 copy)

Navy Radiation Technology, Air Force Weapons Lab (NLO), Kirtland AFB, NM 87117 (1 copy)

Naval Surface Weapons Center, White Oak, Silver Spring, MD 20910 - Attn: Dr. Leon H. Schindel (Code 310) (1 copy)
Dr. E. Leroy Harris (Code 313) (1 copy)
Mr. K. Enkenhaus (Code 034) (1 copy)
Mr. J. Wise (Code 917) (1 copy)
Technical Library (1 copy)

U.S. Naval Weapons Center, China Lake, CA 93555 - Atn: Technical Library (1 copy)

HQ USAF (AF/RDPS), The Pentagon, Washington, D.C. 20330 - Attn: Lt. Col. A.J. Chiota (1 copy)

HQ AFSC/XRLW, Andrews AFB, Washington, D.C. 20331 - Attn: Maj. J.M. Walton (1 copy)

HQ AFSC (DLCAW), Andrews AFB, Washington, D.C. 20331 - Attn: Maj. H. Axelrod (1 copy)

Air Force Weapons Laboratory, Kirtland AFB, NM 87117 - Attn: LR (1 copy)
AL (1 copy)

HQ SAMSO (XRTD), P.O. Box 92960, Worldway Postal Center, Los Angeles, CA 90009 - Attn: Lt. Dorian DeMaio (XRTD) (1 copy)

AF Avionics Lab (TEO), Wright Patterson AFB, OH 45433 - Attn: Mr. K. Hutchinson (1 copy)

Dept. of the Air Force, Air Force Materials Lab. (AFSC), Wright Patterson AFB, OH 45433 - Attn: Maj. Paul Elder (LPS) (1 copy)
Laser Window Group

HQ Aeronautical Systems Div., Wright Patterson AFB, OH 45433 - Attn: XRF - Mr. Clifford Fawcett (1 copy)

Rome Air Development Command, Griffiss AFB, Rome, NY 13440 - Attn: Mr. R. Urtz (OCSE) (1 copy)

HQ Electronics Systems Div. (ESL), L.G. Hanscom Field, Bedford, MA 01730 - Attn: Mr. Alfred E. Anderson (XRT) (1 copy)
Technical Library (1 copy)

Air Force Rocket Propulsion Lab., Edwards AFB, CA 93523 - Attn: B.R. Bornhorst, (LKCG) (1 copy)

Air Force Aero Propulsion Lab., Wright Patterson AFB, OH 45433 - Attn: Col. Walter Moe (CC) (1 copy)

Dept. of the Air Force, Foreign Technology Division, Wright Patterson AFB, OH 45433 - Attn: PDTN (1 copy)

Commandant of the Marine Corps, Scientific Advisor (Code RD-1), Washington, D.C. 20380 (1 copy)

Aerospace Research Labs., (AP), Wright Patterson AFB, OH 45433 - Attn: Lt. Col. Max Duggins (1 copy)

Defense Intelligence Agency, Washington, D.C. 20301 - Attn: Mr. Seymour Berler (DT1B) (1 copy)

Central Intelligence Agency, Washington, D.C. 20505 - Attn: Mr. Julian C. Nall (1 copy)

Analytic Services, Inc., 5613 Leesburg Pike, Falls Church, VA 22041 - Attn: Dr. John Davis (1 copy)

Aerospace Corp., P.O. Box 92957, Los Angeles, CA 90009 - Attn: Dr. G.P. Millburn (1 copy)

Airesearch Manuf. Co., 9851-9951 Sepulveda Blvd., Los Angeles, CA 90009 - Attn: Mr. A. Colin Stancliffe (1 copy)

Atlantic Research Corp., Shirley Highway at Edsall Road, Alexandria, VA 22314 - Attn: Mr. Robert Naismith (1 copy)

Avco Everett Research Lab., 2385 Revere Beach Parkway, Everett, MA 02149 - Attn: Dr. George Sutton (1 copy)
Dr. Jack Daugherty (1 copy)

Battelle Columbus Laboratories, 505 King Avenue, Columbus, OH 43201 - Attn: Mr. Fred Tietzel (STPIAC) (1 copy)

Bell Aerospace Co., Buffalo, NY 14240 - Attn: Dr. Wayne C. Solomon (1 copy)

Boeing Company, P.O. Box 3999, Seattle, WA 98124 - Attn: Mr. M.1. Gamble (2-, 460, MS 8C-88) (1 copy)

Electro-Optical Systems, 300 N. Halstead, Pasadena, CA 91107 - Attn: Dr. Andrew Jensen (1 copy)

ESL, Inc., 495 Java Drive, Sunnyvale, CA 94086 - Attn: Arthur Einhorn (1 copy)

DISTRIBUTION LIST (Continued)

General Electric Co., Space Division, P.O. Box 8555, Philadelphia, PA 19101 - Attn: Dr. R. V. Siglsmonti (1 copy)

General Electric Co., 100 Plastics Avenue, Pittsfield, MA 01201 - Attn: Mr. D.G. Harrington (Rm. 1044) (1 copy)

General Research Corp., P.O. Box 3587, Santa Barbara, CA 93105 - Attn: Dr. R. Holbrook (1 copy)

General Research Corp., 1501 Wilson Blvd., Suite 700, Arlington, VA 22209 - Attn: Dr. Giles F. Crimi (1 copy)

Hercules, Inc., Industrial System Dept., Wilmington, DE 19899 - Attn: Dr. R.S. Voris (1 copy)

Hercules, Inc., P.O. Box 210, Cumberland, MD 21502 - Attn: Dr. Ralph R. Preckel (1 copy)

Hughes Research Labs., 3011 Malibu Canyon Road, Malibu, CA 90265 - Attn: Dr. D. Forster (1 copy)

Hughes Aircraft Co., Aerospace Group - Systems Division, Canoga Park, CA 91304 - Attn: Dr. Jack A. Alcalay (1 copy)

Hughes Aircraft Co., Centinela and Teale Streets, Bldg. 6, MS E-125, Culver City, CA 90230 - Attn: Dr. William Yates (1 copy)

Institute for Defense Analyses, 400 Army-Navy Drive, Arlington, VA 22202 - Attn: Dr. Alvin Schnitzler (1 copy)

Johns Hopkins University, Applied Physics Lab., 8621 Georgia Avenue, Silver Spring, MD 20910 - Attn: Dr. Albert M. Stone (1 copy)

Lawrence Livermore Laboratory, P.O. Box 808, Livermore, CA 94550 - Attn: Dr. R.E. Kidder (1 copy)
Dr. E. Teller (1 copy)
Dr. Joe Fleck (1 copy)

Los Alamos Scientific Laboratory, P.O. Box 1663, Los Alamos, NM 87544 - Attn: Dr. Keith Boyer (1 copy)

Lulejian and Associates, Inc., Del Amo Financial Center, 21515 Hawthorne Blvd. - Suite 500, Torrance, CA 90503 (1 copy)

Lockheed Palo Alto Res. Lab., 3251 Hanover St., Palo Alto, CA 94303 - Attn: L.R. Lunsford, Orgn. 52-24, Bldg. 201 (1 copy)

Mathematical Sciences Northwest, Inc., P.O. Box 1887, Bellevue, WN 98009 - Attn: Dr. Abraham Hertzberg (1 copy)

Martin Marietta Corp., P.O. Box 179, Mail Station 0471, Denver, CO 80201 - Attn: Mr. Stewart Chapin (1 copy)

Massachusetts Institute of Technology, Lincoln Laboratory, P.O. Box 73, Lexington, MA 02173 - Attn: Dr. S. Edelberg (1 copy)
Dr. L.C. Marquet (1 copy)

McDonnell Douglas Astronautics Co., 5301 Bolsa Avenue, Huntington Beach, CA 92647 - Attn: Mr. P.L. Klevatt, Dept. A3-830-BBFO, M/S 9 (1 copy)

McDonnell Douglas Research Labs., Dept. 220, Box 516, St. Louis, MO 63166 - Attn: Dr. D.P. Ames (1 copy)

MITRE Corp., P.O. Box 208, Bedford, MA 01730 - Attn: Mr. A.C. Cron (1 copy)

North American Rockwell Corp., Autonetics Div., Anaheim, CA 92803 - Attn: Mr. T.T. Kumagi, C/476 Mail Code HA18 (1 copy)

Northrop Corp., 3401 West Broadway, Hawthorne, CA 90250 - Attn: Dr. Gerard Hasserjian, Laser Systems Dept. (1 copy)

Dr. Anthony N. Pirri, Physical Sciences, Inc., 18 Lakeside Office Park, Wakefield, MA 01880 (1 copy)

RAND Corp., 1700 Main Street, Santa Monica, CA 90406 - Attn: Dr. C.R. Culp/Mr. C.A. Carter (1 copy)

Raytheon Co., 28 Seyon Street, Waltham, MA 02154 - Attn: Dr. F.A. Horrigan (Res. Div.) (1 copy)

Raytheon Co., Boston Post Road, Sudbury, MA 01776 - Attn: Dr. C. Sonnenschien (Equip. Div.) (1 copy)

Raytheon Co., Bedford Labs, Missile Systems Div., Bedford, MA 01730 - Attn: Dr. H.A. Mehlhorn (1 copy)

Riverside Research Institute, 80 West End Street, New York, NY 10023 - Attn: Dr. L.H. O'Neill (1 copy)
Dr. John Bose (1 copy)
(HPECL Library) (1 copy)

R&D Associates, Inc., P.O. Box 3580, Santa Monica, CA 90431 - Attn: Dr. R.E. LeLevier (1 copy)

Rockwell International Corporation, Rocketdyne Division, Albuquerque District Office, 3636 Menaul Blvd., NE, Suite 211, Albuquerque, NM 87110 - Attn: C.K. Kraus, Mgr. (1 copy)

SANDIA Corp., P.O. Box 5800, Albuquerque, NM 87115 - Attn: Dr. Al Narath (1 copy)

Stanford Research Institute, Menlo Park, CA 94025 - Attn: Dr. F.T. Smith (1 copy)

Science Applications, Inc., 1911 N. Ft. Meyer Drive, Arlington, VA 22209 - Attn: L. Peckam (1 copy)

Science Applications, Inc., P.O. Box 328, Ann Arbor, MI 48103 - Attn: R.E. Meredith (1 copy)

Science Applications, Inc., 6 Preston Court, Bedford, MA 01703 - Attn: R. Greenberg (1 copy)

Science Applications, Inc., P.O. Box 2351, La Jolla, CA 92037 - Attn: Dr. John Asmus (1 copy)

Systems, Science and Software, P.O. Box 1620, La Jolla, CA 92037 - Attn: Alan F. Klein (1 copy)

Systems Consultants, Inc., 1050 31st Street, NW, Washington, D.C. 20007 - Attn: Dr. R.B. Keller (1 copy)

Thiokol Chemical Corp., WASATCH Division, P.O. Box 524, Brigham City, UT 84302 - Attn: Mr. J.E. Hansen (1 copy)

TRW Systems Group, One Space Park, Bldg. R-1, Rm. 1050, Redondo Beach, CA 90278 - Attn: Mr. Norman Campbell (1 copy)

United Technologies Research Center, 400 Main Street, East Hartford, CT 06108 - Attn: Mr. C.H. McLafferty (3 copies)

DISTRIBUTION LIST (Continued)

United Technologies Research Center, Pratt and Whitney Aircraft Div., Florida R&D Center, West Palm Beach, FL 33402 Attn: Dr. R. A. Schmidtke (1 copy)
Mr. Ed Pinsley (1 copy)

VARIAN Associates, EIMAC Division, 301 Industrial Way, San Carlos, CA 94070 - Attn: Mr. Jack Quinn (1 copy)

Vought Systems Division, LTV Aerospace Corp., P.O. Box 5907, Dallas, TX 75222 - Attn: Mr. F. G. Simpson, MS 254142 (1 copy)

Westinghouse Electric Corp., Defense and Space Center, Balt-Wash. International Airport - Box 746, Baltimore, MD 21203 - Attn: Mr. W. F. List (1 copy)

Westinghouse Research Labs., Beulah Road, Churchill Boro, Pittsburgh, PA 15235 - Attn: Dr. E. P. Riedel (1 copy)

United Technologies Research Center, East Hartford, CT 06108 - Attn: A. J. DeMaria (1 copy)

Airborne Instruments Laboratory, Walt Whitorian Road, Melville, NY 11746 - Attn: F. Pace (1 copy)

General Electric R&D Center, Schenectady, NY 12305 - Attn: Dr. Donald White (1 copy)

Cleveland State University, Cleveland, OH 44115 - Attn: Dean Jack Soules (1 copy)

EXXON Research and Engineering Co., P.O. Box 8, Linden, NJ 07036 - Attn: D. Grafstein (1 copy)

University of Maryland, Department of Phyalcs and Astronomy, College Park, MD 20742 - Attn: D. Currie (1 copy)

Sylvania Electric Products, Inc., 100 Fergeson Drive, Mountain View, CA 94040 - Attn: L. M. Osterink (1 copy)

North American Rockwell Corp., Autonetica Division, 3370 Miraloma Avenue, Anaheim, CA 92803 - Attn: R. Gudmundsen (1 copy)

Massachusetts Institute of Technology, 77 Massachusetts Avenue, Cambridge, MA 02138 - Attn: Prof. A. Javan (1 copy)

Lockheed Missile & Space Co., Palo Alto Research Laboratories, Palo Alto, CA 94304 - Attn: Dr. R. C. Ohlman (1 copy)

ILC Laboratories, Inc., 164 Commercial Street, Sunnyvale, CA 94086 - Attn: L. Noble (1 copy)

University of Texas at Dallas, P.O. Box 30365, Dallas, TX 75230 - Attn: Prof. Carl B. Collins (1 copy)

Polytechnic Institute of New York, Rt. 110, Farmingdale, NY 11735 - Attn: Dr. William T. Walter (1 copy)